Figure S1. Zhu et al.

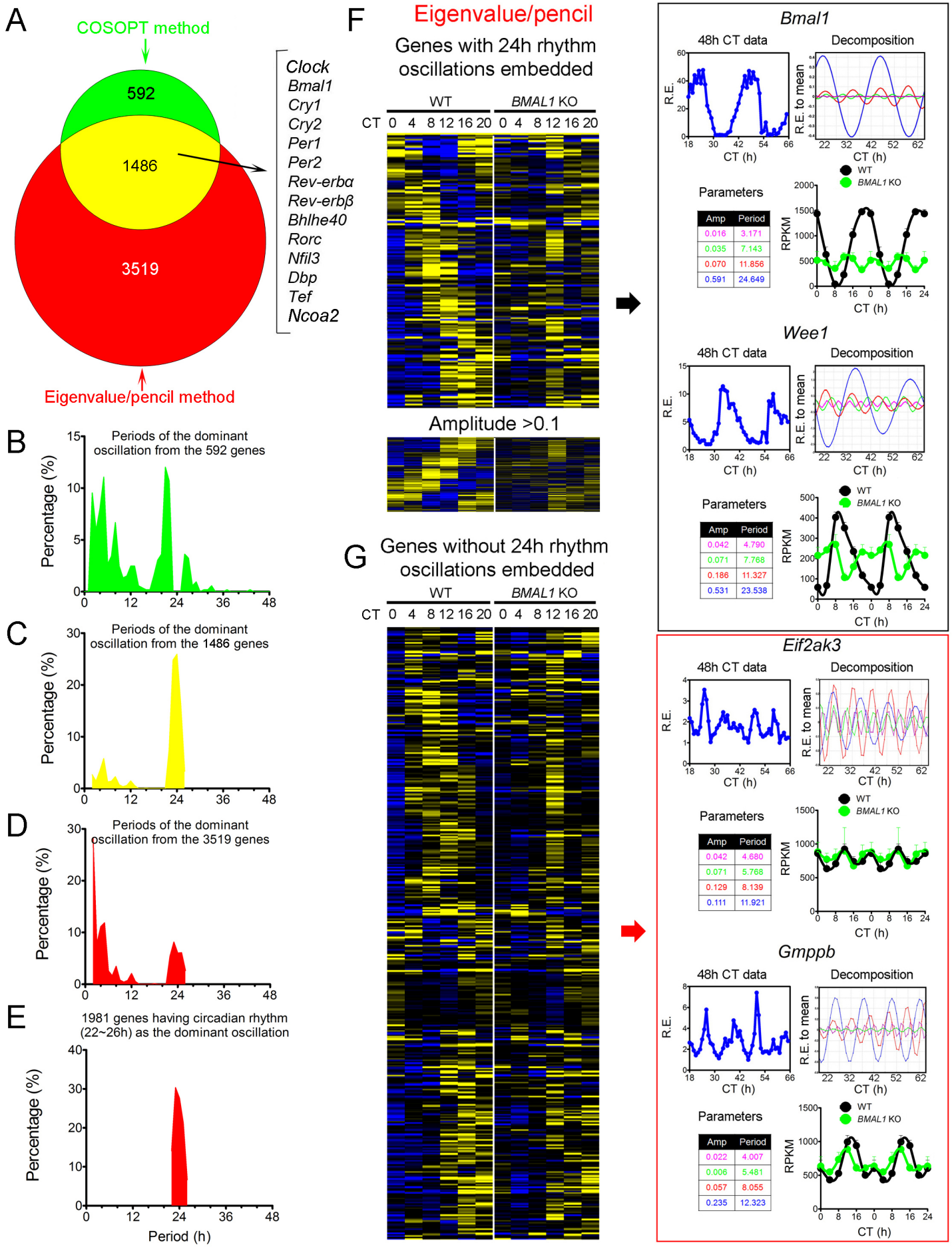

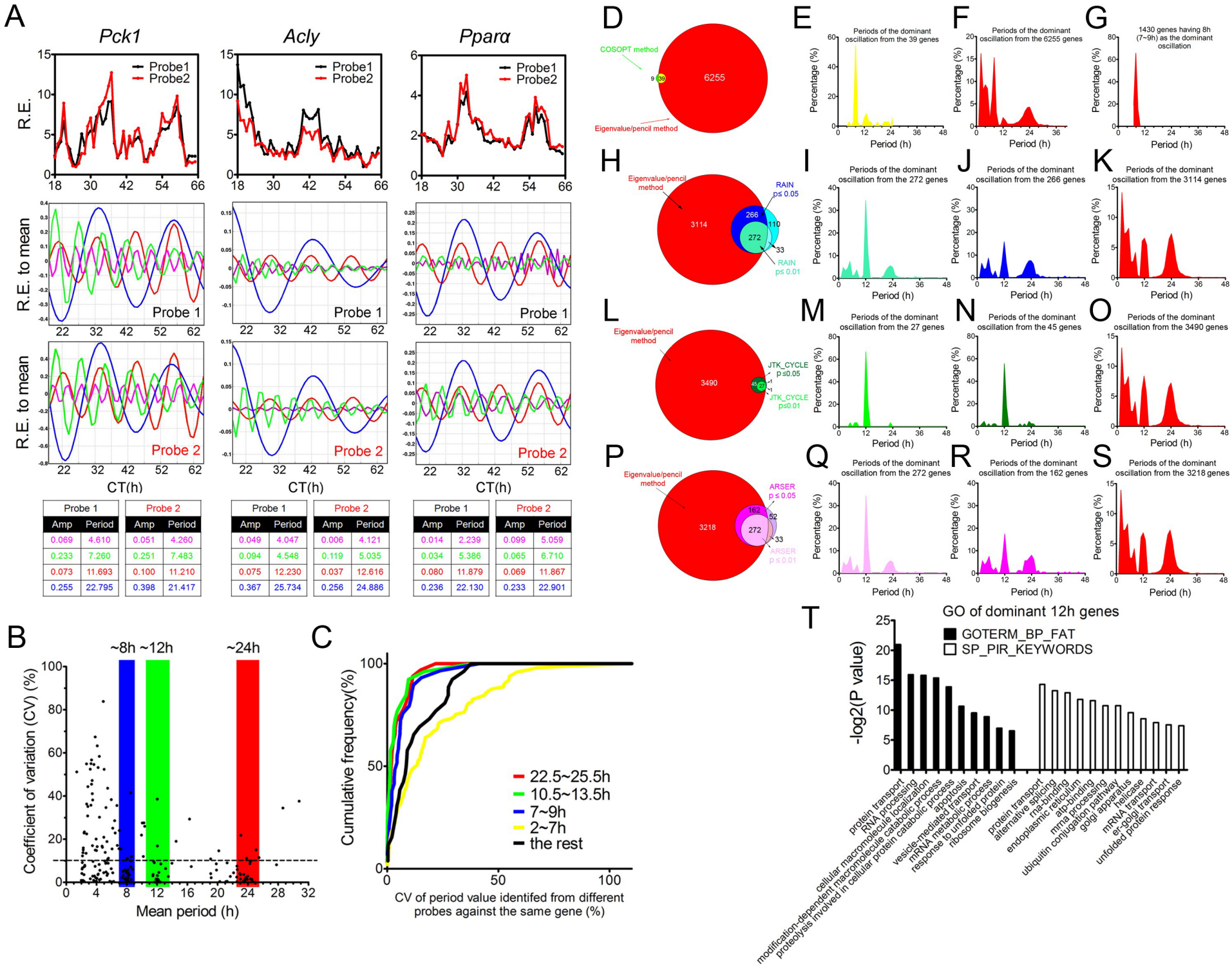

Probe 1		Probe 2	
Amp	Period	Amp	Period
0.069	4.610	0.051	4.260
0.233	7.260	0.251	7.483
0.073	11.693	0.100	11.210
0.255	22.795	0.398	21.417

Probe 1		Probe 2	
Amp	Period	Amp	Period
0.049	4.047	0.006	4.121
0.094	4.548	0.119	5.035
0.075	12.230	0.037	12.616
0.367	25.734	0.256	24.886

Probe 1		Probe 2	
Amp	Period	Amp	Period
0.014	2.239	0.099	5.059
0.034	5.386	0.065	6.710
0.080	11.879	0.069	11.867
0.236	22.130	0.233	22.901

Figure S2.Zhu et al.

Figure S3. Zhu et al.

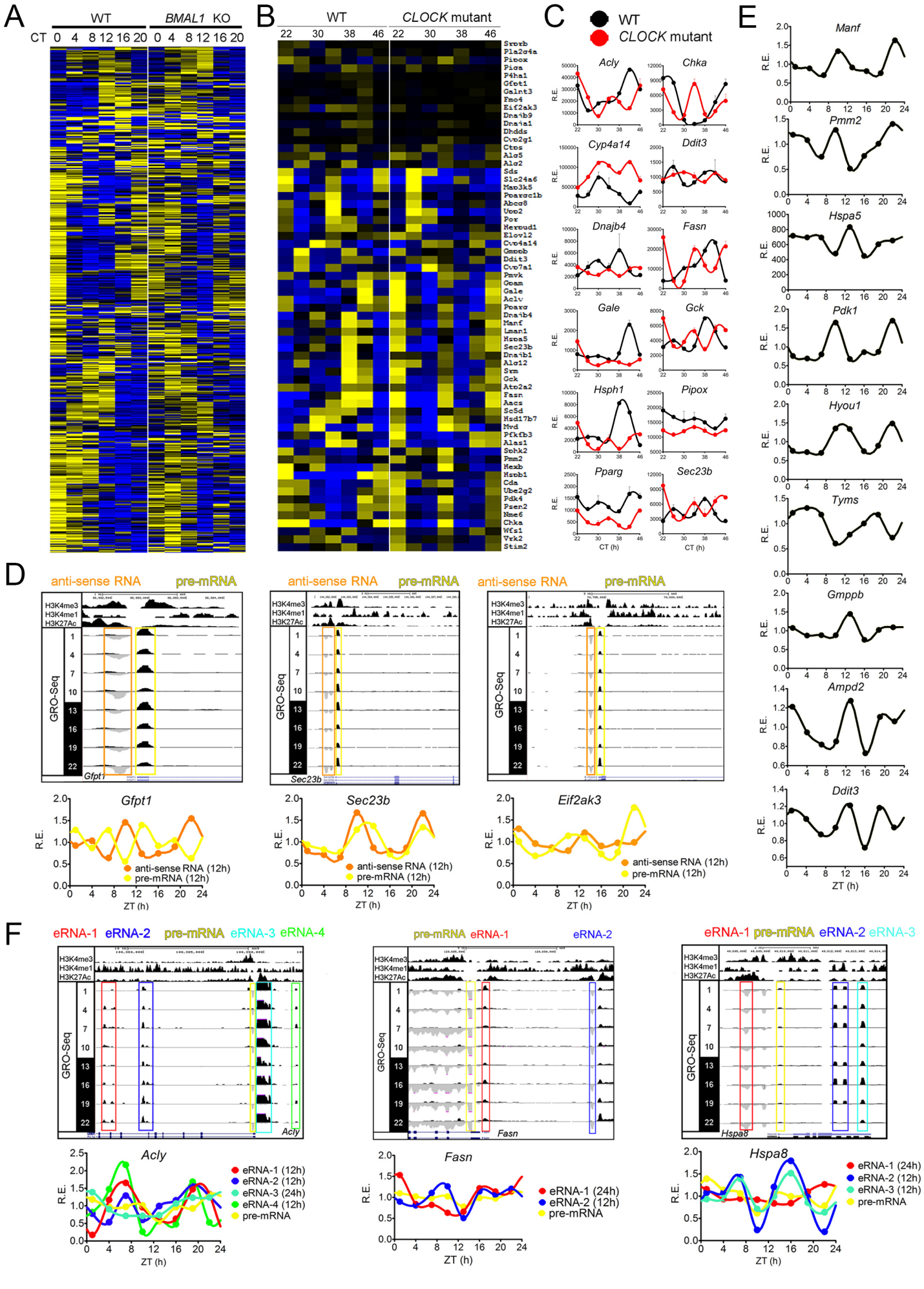

Figure S4. Zhu et al.

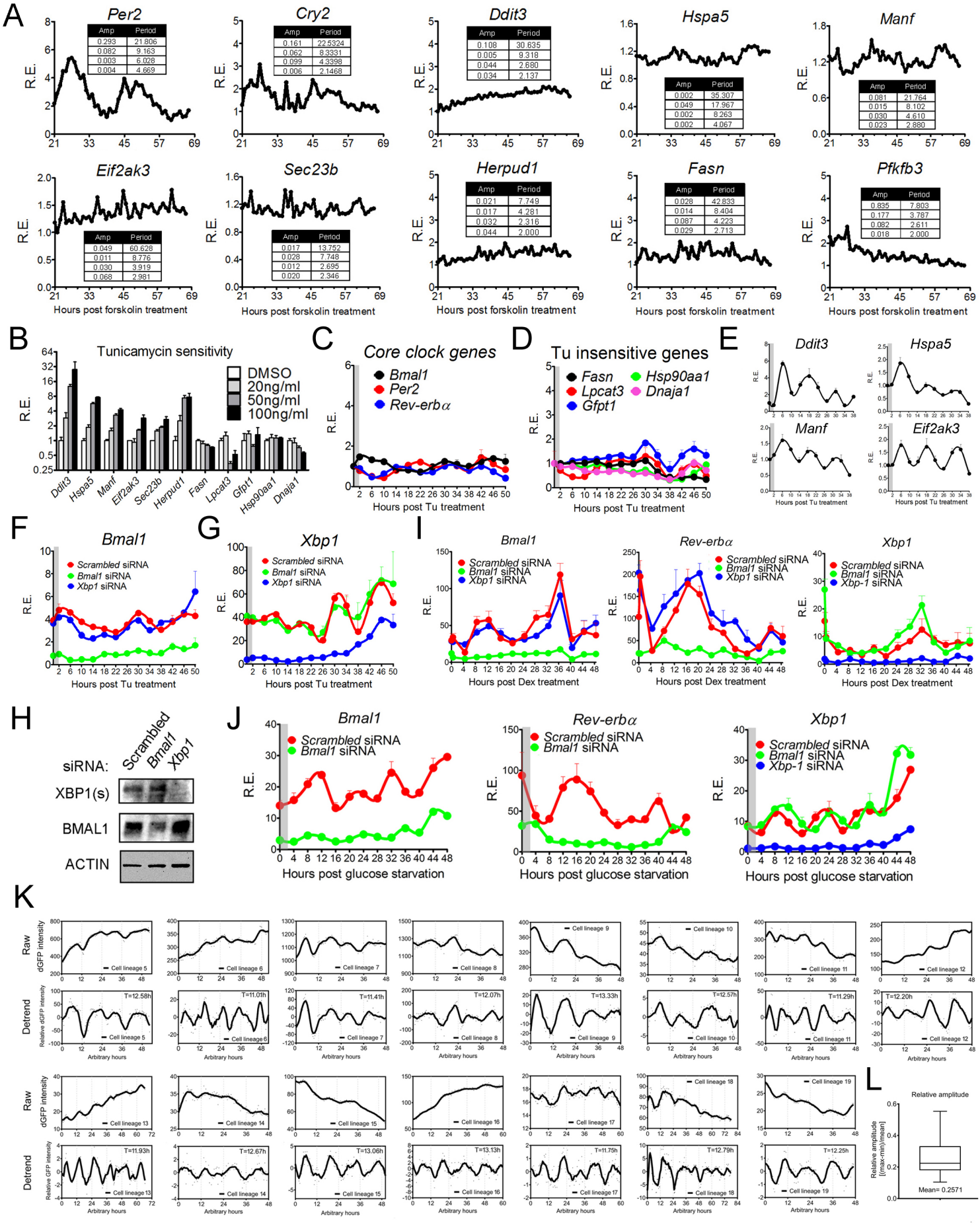

Figure S5. Zhu et al.

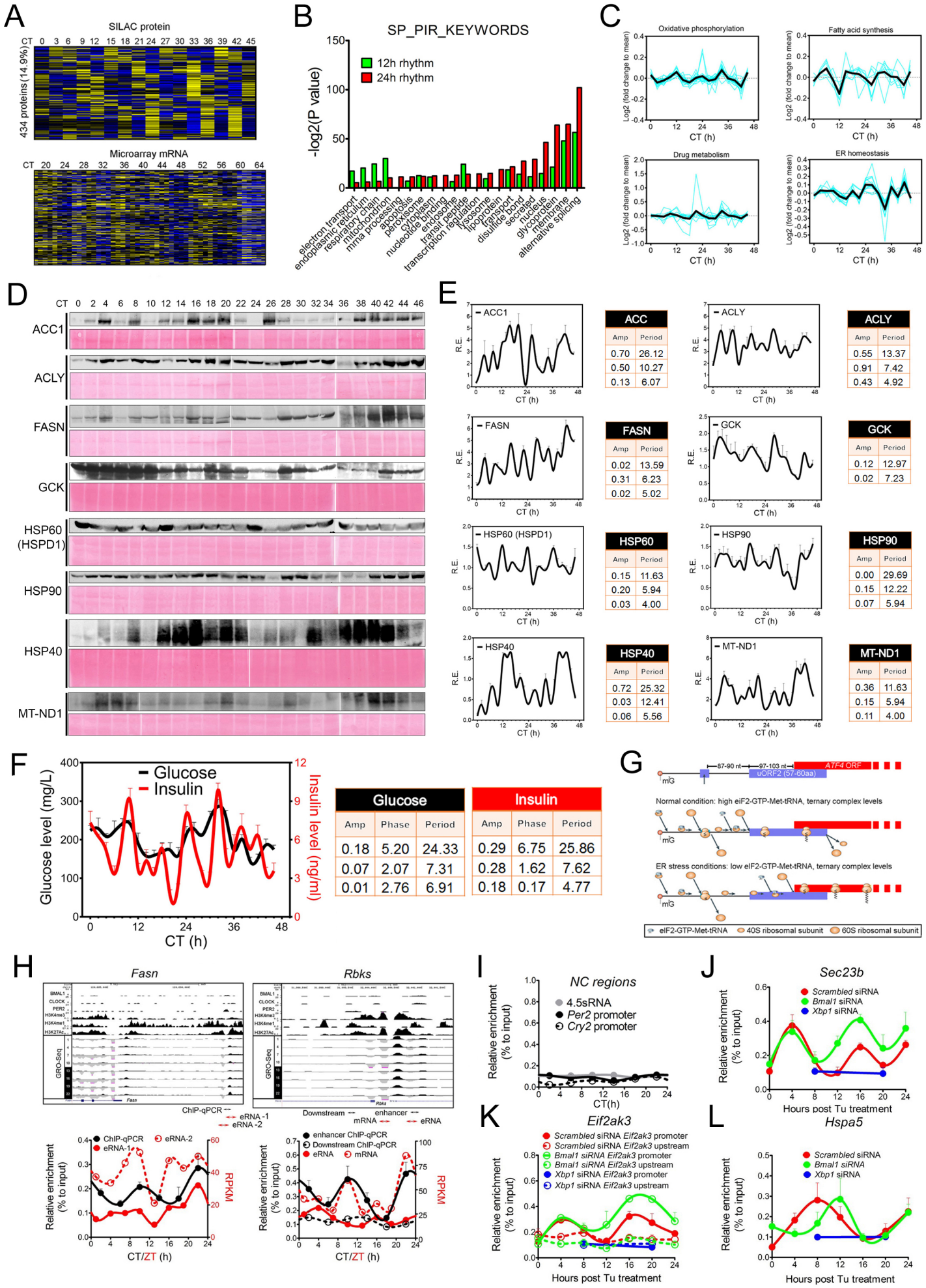

Figure S6. Zhu et al.

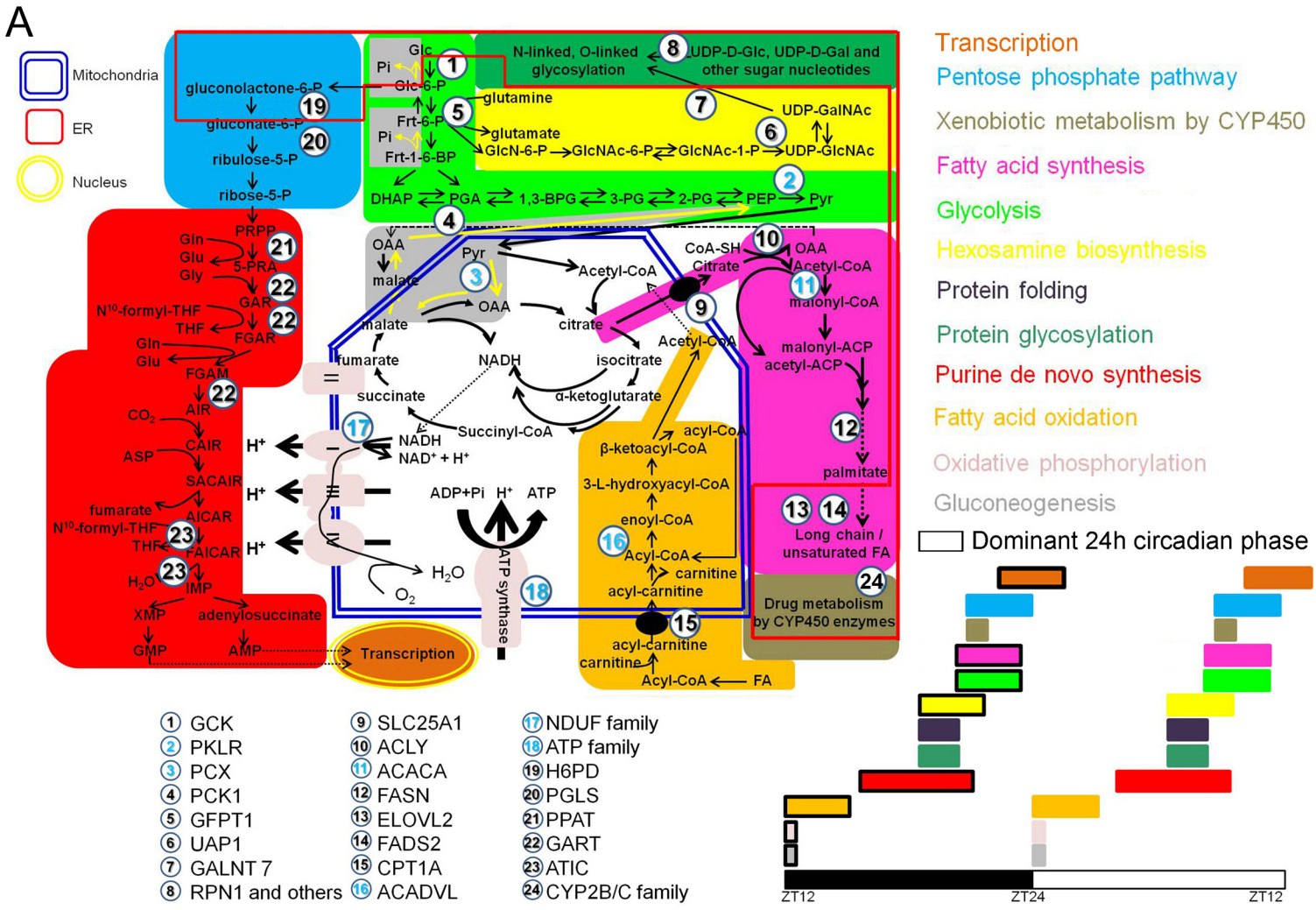

B

RBKS

ATP + D-ribose ↔ ADP + D-ribose 5-phosphate

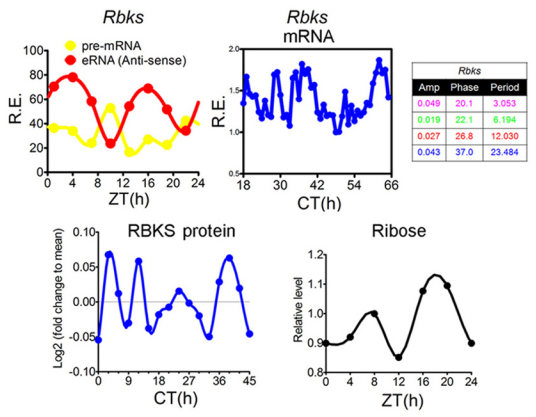

Rbks		
Amp	Phase	Period
0.049	20.1	3.053
0.019	22.1	6.194
0.027	26.8	12.030
0.043	37.0	23.484

C

SUCLA2

Succinyl CoA + Pi + NDP ↔ Succinate + CoA + NTP

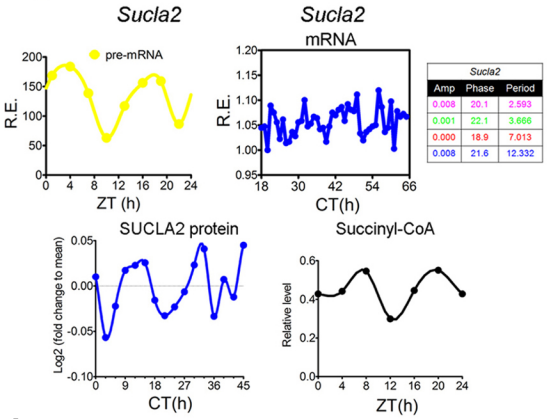

Sucla2		
Amp	Phase	Period
0.008	20.1	2.593
0.001	22.1	3.666
0.000	18.9	7.013
0.008	21.6	12.332

D

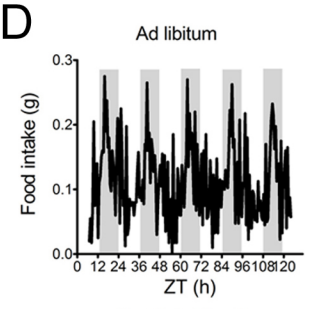

E

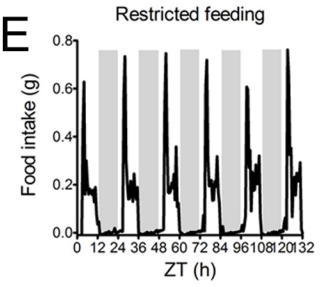

F

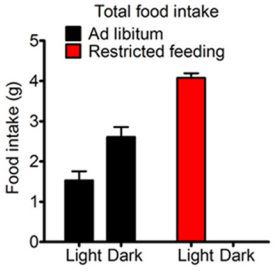

G

Mouse #1	
Amp	Period
0.0012	1.852
0.0196	11.803
0.0228	25.276
0.8295	mean

Mouse #2	
Amp	Period
0.0178	1.442
0.0004	2.250
0.0062	12.412
0.0193	24.196
0.8622	mean

Mouse #3	
Amp	Period
0.0060	2.303
0.0095	2.873
0.0190	11.815
0.0248	24.744
0.8495	mean

Mouse #4	
Amp	Period
0.0030	2.171
0.0002	6.568
0.0045	10.599
0.0424	23.761
0.8625	mean

Mouse #5	
Amp	Period
0.0004	1.405
0.0065	1.831
0.0065	12.142
0.0310	24.128
0.0033	58.888
0.8677	mean

Mouse #6	
Amp	Period
0.0027	3.613
0.0012	7.850
0.0064	11.720
0.0238	23.914
0.8931	mean

Mouse #7	
Amp	Period
0.0020	5.009
0.0120	8.409
0.0085	12.481
0.0238	24.696
0.9080	mean

H

Mouse #1	
Amp	Period
0.0037	4.828
0.0116	7.424
0.0256	7.996
0.0010	20.277
0.0817	23.926
0.8843	mean

Mouse #2	
Amp	Period
0.0112	4.795
0.0078	6.020
0.0196	7.990
0.0072	12.380
0.0866	23.840
0.8913	mean

Mouse #3	
Amp	Period
0.0090	3.453
0.0093	4.792
0.0081	6.096
0.0170	7.973
0.0722	23.830
0.8941	mean

Mouse #4	
Amp	Period
0.0076	3.438
0.0131	5.998
0.0151	7.942
0.0185	12.204
0.0904	23.770
0.9236	mean

Mouse #5	
Amp	Period
0.0083	4.821
0.0102	5.999
0.0220	7.962
0.0841	23.857
0.0080	55.522
0.8897	mean

Mouse #6	
Amp	Period
0.0085	3.427
0.0099	5.983
0.0149	7.954
0.0283	12.435
0.0891	23.819
0.9412	mean

Mouse #7	
Amp	Period
0.0080	3.440
0.0038	4.053
0.0089	5.991
0.0190	8.018
0.0899	24.061
0.9412	mean

Mouse #8	
Amp	Period
0.0057	4.792
0.0067	6.003
0.0206	8.031
0.0094	12.034
0.0866	24.030
0.8936	mean

Figure S7. Zhu et al

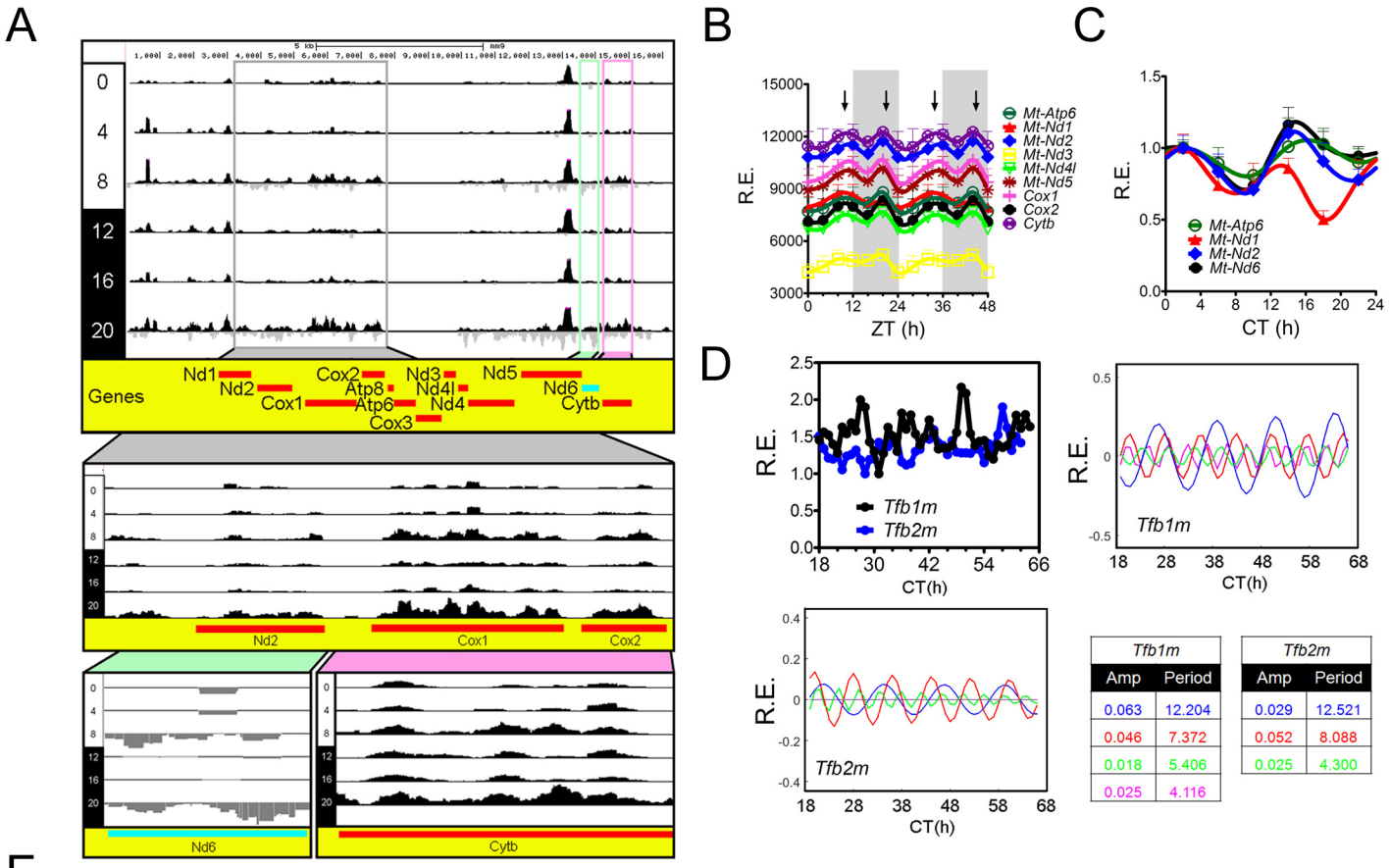

Tfb1m	
Amp	Period
0.063	12.204
0.046	7.372
0.018	5.406
0.025	4.116

Tfb2m	
Amp	Period
0.029	12.521
0.052	8.088
0.025	4.300

E

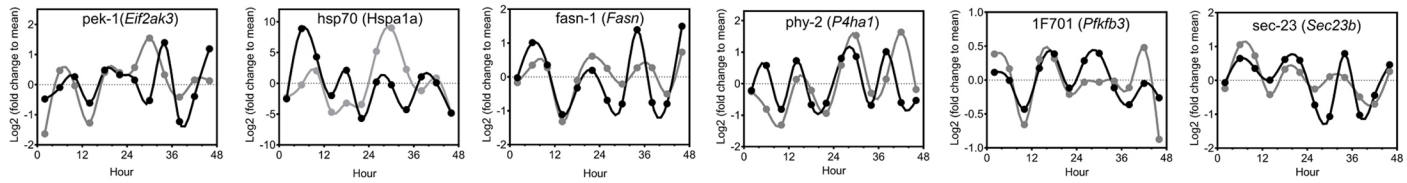

F

Top ~12h cycling gene identified in mouse liver

Gene names in mouse	Period	Relative amplitude	Ortholog gene in C. elegans	Having ~12h rhythmicity in C. elegans?
Rgs16	10.680	1.085	rgs-7	Yes
Nipal1	11.758	0.790	nipa-1	Yes
Hspa1b	11.823	0.785	hsp-70	Yes
Bag3	11.594	0.667	wwp-1	Yes
Nr1d1	11.532	0.653	nhr-85	No
Mfsd2a	11.267	0.604	XF291	No
Tsku	11.340	0.584	tol-1	Yes
Cwf19l2	11.197	0.569	B0361.2	Yes
Dbp	11.647	0.520	ces-2	No
Fasn	12.711	0.518	fasn-1	Yes
Usp2	11.271	0.484	4H525	Yes

G

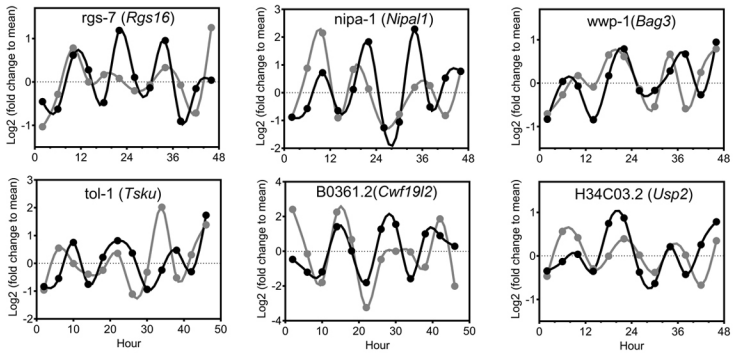

H

Top circadian gene identified in mouse liver

Gene names in mouse	Period	Relative amplitude	Ortholog gene in C. elegans	Having circadian rhythmicity in C. elegans?
Mfsd2a	22.615	1.448	XF291	No
Usp2	23.260	1.159	4H525	No
Lrp1	24.142	1.155	lrp-2	No
Ccrn4l	23.031	1.084	ccr-4	No
Dbp	23.396	1.081	ces-2	Yes for one rep
Nr1d1	23.283	0.993	nhr-85	No
AW107722	22.799	0.984	not found	N/A
Lpin1	23.235	0.975	lpin-1	No
Gm129	23.321	0.950	not found	N/A
E030016H06Rik	24.856	0.877	not found	N/A

I

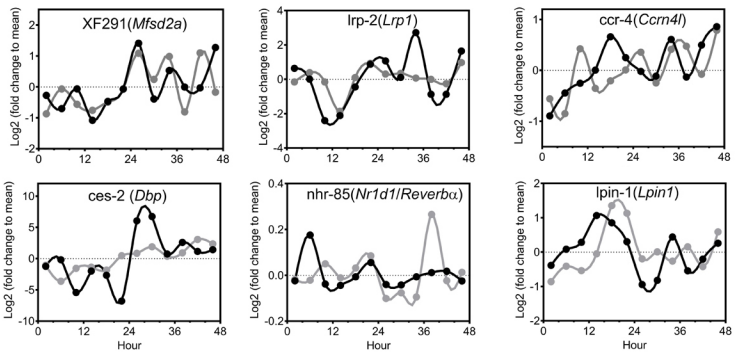

SUPPLEMENTAL FIGURES:

Figure S1. The eigenvalue/pencil method can robustly identify circadian genes, related to Figure 1.

(A) Venn diagram comparison of the number of circadian genes identified via the eigenvalue/pencil or the COSOPT method described in (Hughes et al., 2009). Core clock genes were identified by both methods. **(B-E)** The distributions of the periods of the dominant oscillations from the 592 circadian genes only identified by the COSOPT method **(B)**, the 1,486 commonly found circadian genes **(C),** the 3,519 circadian genes only identified by the eigenvalue approach **(D)** or the dominant 1,981 circadian genes identified by the eigenvalue approach (**E**). **(F,G)** All 18,108 genes analyzed by the eigenvalue/pencil method are divided in two groups based upon the presence **(F)** or absence **(G)** of superimposed ~24h oscillations. For mRNA with embedded ~24h oscillations, those with the relative amplitude of 24h oscillation larger than 0.1 are further selected. Heatmaps of mRNA expression in wild-type (WT) or *BMAL1*$^{-/-}$ (*BMAL1* KO) mice from a published RNA-Seq database at different CTs (Yang et al., 2016) are shown. Further, raw microarray data used for deconvolution, deconvoluted plots, identified parameters for different oscillations and mRNA expression of representative genes (*Bmal1* and *Wee1* represent genes with 24h oscillation and *Eif2ak3* and *Gmppb* represent genes without 24h oscillation in WT mice) in wild-type (WT) or *BMAL1* knock-out (*KO*) mice are shown on the right (n=4). The RNA-Seq data are double plotted for better visualization.

Figure S2. Eigenvalue/pencil approach identifies wide prevalence of 8h and 12h hepatic genes, which are robust oscillations, related to Figure 1.

(A-C) To tested the robustness of the identified oscillations, we compared the oscillations derived from different microarray probes against the same gene. A 60-gene cassette containing multiple microarray probes per gene (Hughes et al., 2009) was randomly selected and subjected to mathematical decomposition. We reasoned that if oscillations from a given gene were robust, then the identified period lengths should be similar, that is with smaller coefficient of variation (CV), among different probe datasets. Likewise,

identified oscillations of largely disparate periods (larger CV value) from different probes are likely to stem from technical noise and are less likely to represent real biological oscillations. Using this rationale, we found that 8h, 12h and 24h are the most robust oscillations as approximately 90% of these oscillations have CV values less than 0.1 **(A-C).** In contrast, oscillations with periods in between (60% with CV <0.1) and with shorter periods (<7h) (only 45% with CV<0.1) were found to be less robust **(A-C)**. Combined with the observation that oscillations of larger periods (8~24h) remain mostly unchanged as more oscillations are added by using higher reduced models (See Supplemental Experimental Procedures), we showed that in addition to the well-characterized circadian rhythm, oscillations with periods of 12h and 8h are robust rhythms with potential biological significance. Detailed figure legends: **(A)** Representative deconvolution of metabolism (*Pck1*, *Acly*, *Pparα*) genes mRNA expression by the eigenvalue/pencil method. For every gene, mRNA expressions detected by two different probe sets are analyzed by the eigenvalue/pencil method. Top row represents raw microarray data (Hughes et al., 2009); second and third rows plot revealed superimposed oscillations for different probe sets; and the fourth row illustrates the amplitudes and periods of different oscillations for different probe sets with the color matching the different oscillations depicted in the second and third row. **(B)** Coefficient of variation (CV) values of period is plotted against the mean period value for every oscillation identified from two or three microarray probe sets against the same gene. **(C)** Cumulative frequencies of period CV for oscillations with different periods calculated from **(B)**. **(D-G)** Comparison of the 8h cycling genes uncovered by the eigenvalue/pencil and the COSOPT method (Hughes et al., 2009). Venn diagram comparison of the number of 8h cycling genes identified via the eigenvalue/pencil or the COSOPT method **(D)**, the distributions of the periods of the dominant oscillations from the 39 commonly found 8h cycling genes **(E)**, the 6,255 8h genes only identified by the eigenvalue approach **(F)** or the dominant 1,430 8h genes identified by the eigenvalue approach (**G**). **(H-I)** Comparison of the 12h cycling genes uncovered by the eigenvalue/pencil and the RAIN method (Thaben and Westermark, 2014). Venn diagram comparison of the number of 12h cycling genes identified via the eigenvalue/pencil or the RAIN method with two p value cut-offs **(H)**, the distributions of the periods of the dominant oscillations from the 272 commonly found 12h cycling genes

with a p value cut-off of 0.01 **(I)**, the 266 commonly found 12h cycling genes with a p value cut-off of 0.05 **(J)** or the dominant 3,114 12h genes only identified by the eigenvalue approach (**K**). **(L-O)** Comparison of the 12h cycling genes uncovered by the eigenvalue/pencil and the JTK_CYCLE method (Hughes et al., 2010). Venn diagram comparison of the number of 12h cycling genes identified via the eigenvalue/pencil or the JTK_CYCLE method with two p value cut-offs **(L)**, the distributions of the periods of the dominant oscillations from the 27 commonly found 12h cycling genes with a p value cut-off of 0.01 **(M)**, the 45 commonly found 12h cycling genes with a p value cut-off of 0.05 **(N)** or the dominant 3,490 12h genes only identified by the eigenvalue approach (**O**). **(P-S)** Comparison of the 12h cycling genes uncovered by the eigenvalue/pencil and the ARSER method (Yang and Su, 2010). Venn diagram comparison of the number of 12h cycling genes identified via the eigenvalue/pencil or the ARSER method with two p value cut-offs **(P)**, the distributions of the periods of the dominant oscillations from the 272 commonly found 12h cycling genes with a p value cut-off of 0.01 **(Q)**, the 162 commonly found 12h cycling genes with a p value cut-off of 0.05 **(R)** or the dominant 3,218 12h genes only identified by the eigenvalue approach (**S**). **(T)** GO analyses revealing top-enriched SP_PIR_KEYWORDS and GOTERM_BP_FAT terms in the 760 dominant 12h genes.

Figure S3. 12h oscillations are transcriptionally-regulated independently from the 24h circadian rhythms in mouse liver, related to Figure 2.

(A) Heatmap of RPKM normalized mRNA expression for genes without embedded ~12h oscillations in wild-type mice in wild-type (WT) or *BMAL1*$^{-/-}$ (*BMAL1* KO) mice from a published RNA-Seq database at different CTs (Yang et al., 2016). **(B,C)** Heatmap **(B)** and representative mRNA expression **(C)** from wild-type (WT) and *CLOCK* mutant (Clockm) mice under constant darkness conditions calculated from a published micro-array database (Miller et al., 2007) and graphed as the mean ± SEM (n = 2). **(D-F)** We sought further evidence for the independence of 12h rhythmicity of gene expression from the circadian rhythm by examining global run-on sequencing (GRO-Seq) data in mouse liver across one diurnal cycle (Fang et al., 2014). GRO-Seq not only can accurately quantify nascent mRNA transcription, but also can identify actively transcribing enhancer

RNAs (eRNA), the level of which closely correlates with neighboring mRNA expression (Lam et al., 2014). We first confirmed that the 12h rhythm of mRNA expression is regulated at the transcription level **(D, E)**. Next, we reasoned that if the 12h rhythm is transcriptionally regulated independently from the circadian rhythm as speculated, we should identify examples of spatial segregation of 12h and 24h cycling eRNAs in the enhancer regions of the same gene that has both 24h and 12h oscillations superimposed at the mRNA level. As expected, we found examples of spatial segregation of 12h and 24h cycling eRNAs in *Acly*, *Fasn* and *Hspa8* genes, all of which have both 24h and 12h oscillations at the mature mRNA level **(F).** Detailed figure legends: RPKM normalized quantification of mouse hepatic RNA synthesis rate under a 12h L/D schedule calculated from a published Gro-Seq database (Fang et al., 2014). UCSC genome browser snapshots of H3K4me3, H3K4me1 and H3K27Ac levels (Koike et al., 2012) as well as Gro-Seq tracks from ZT1 to ZT22 at three-hour intervals are provided at the top. **(D)** UCSC genome browser snapshots (top) and quantification of the Gro-Seq signal of the RNA transcribed from the sense (pre-mRNA) and anti-sense (anti-sense RNA) strand of *Gfpt1*, *Sec23b* and *Eif2ak3* gene (bottom). Boxes indicate regions of RNA used for quantification. **(E)** Normalized quantification of additional 12h cycling mouse hepatic pre-mRNA level under a 12h L/D schedule. **(F)** UCSC genome browser snapshots of H3K4me3, H3K4me1 and H3K27Ac levels (Koike et al., 2012) as well as Gro-Seq tracks from ZT1 to ZT22 at three-hour intervals and quantification of the Gro-Seq signal of the pre-mRNAs and eRNAs transcribed from *Acly*, *Fasn* and *Hspa8* gene loci. Boxes indicate regions of RNA used for quantification.

Figure S4. Circadian clock-independent 12h rhythmicity of gene expression can be synchronized by the metabolic/ER stress cues, related to Figure 3 and 4.

(A) Raw microarray data and eigenvalue/pencil decomposition of 10 genes in forskolin-synchronized NIH3T3 cells (Hughes et al., 2009). **(B)** MEFs were treated with various doses of Tu for 2h and qPCR was performed on different genes 4h later. **(C, D)** MEFs were treated with Tu (25ng/ml) for 2h and qPCR was performed at different time points post-Tu shock. **(E)** MEFs were treated with a lower dose of Tu (15ng/ml) for 2h and qPCR was performed at different time points post-Tu shock. **(F, G)** MEFs were transfected with

different siRNAs and treated with Tu (25ng/ml) for 2h and qPCR was performed at different time points post-Tu shock for *Bmal1* **(F)** and *Xbp1* **(G)** genes. **(H)** Immunoblot analysis of BMAL1 and XBP1s in MEFs transfected with different siRNAs before Tu or GD treatment. **(I)** MEFs were transfected with different siRNAs and treated with Dex (100nM) for 30min and qPCR was performed at different time points post-Dex shock. (**J**) MEFs were transfected with different siRNAs and glucose starved for 2h and qPCR was performed at different time points post-GD. Gray boxes indicate the duration of Tu shock or GD. (**K**) Quantifications of both raw and polynomial-detrended single cell lineage recordings. (**L**) Calculated relative amplitudes of single cell oscillations with dominant periods between 11 to 14h. Data are graphed as the mean ± SEM (n=3).

Figure S5. XBP1s transcriptionally regulates the mammalian 12h clock., related to Figure 5.

(A) Heatmaps of proteins exhibiting 12h oscillation in mouse liver generated from a published SILAC database (Robles et al., 2014) (top) and of corresponding mRNA expression (Hughes et al., 2009) (bottom) at different CTs. **(B)** GO analysis revealing top-enriched SP_PIR_KEYWORDS in 12h and 24h cycling proteins. **(C)** Log_2 mean normalized level of proteins with a 12h period oscillation in mouse liver generated from a published SILAC database involved in different biological pathways (Robles et al., 2014). **(D-F)** Mice were entrained under 12L:12D schedule for 14 days before released into constant darkness. 36 hours later, mice were sacrificed at a 2h interval for a total of 48h. Representative western blot analysis from liver whole cell lysates **(D)** and quantification and eigenvalue/pencil decomposition **(E)** of key hepatic metabolic enzymes (n=3). **(F)** Quantification and eigenvalue/pencil decomposition of plasma insulin and glucose oscillations during the 48h period (n=3). Please note that both plasma glucose and insulin levels reveal robust circadian rhythmicity, with phases consistent with previously published results (Wang et al., 2011; Zhu et al., 2015). In addition, we observed an 1.55h phase delay between insulin and glucose oscillation, consistent with the kinetics of insulin release after an increase in blood glucose levels (Gerich, 2002). Intriguingly, neither plasma glucose nor insulin oscillations exhibited 12h rhythmicity. Further, insulin oscillation showed a more “pulsatile” pattern, consisting of superimposed oscillations with

periods of ~24h, 8h and 5h of relatively similar amplitudes; while the glucose oscillation is subtler with a strong circadian rhythmicity. The “pulsatile” insulin oscillating pattern across a diurnal cycle may be a macroscopic manifestation of 5~15min periodic insulin release (Porksen et al., 2002). These data indicate that mice kept under constant darkness conditions maintain a rhythmic feeding-fasting cycle. **(G)** Diagram of translational control of ATF4 under normal and ER stress conditions. Translation of the mammalian activating transcription factor-4 (ATF4) is regulated by two uORFs. When the eIF2-GTP-Met-tRNA ternary complex is abundant (in the presence of low levels of eIF2α phosphorylation) under normal conditions, the ribosomes initiate at uORF1 and frequently reinitiate at uORF2. As uORF2 overlaps with the ATF4 ORF, the translation of uORF2 suppresses the translation of ATF4. During ER stress, when the level of the ternary complex is reduced, the ribosome scans through uORF2 and initiates at the ATF4 initiation codon. Coding regions are shown as red rectangles, uORFs are shown as purple rectangles, ribosomes are shown in orange circles (60S subunit, large circle; 40S subunit, small circle). The ternary complex is shown as light blue circle. m^7G, cap structure. **(H)** Hepatic XBP1s binding to regulatory regions of key 12h metabolic genes under constant darkness conditions assayed by ChIP-qPCR (n=3~4) overlaid with RPKM normalized quantification of mouse hepatic RNA synthesis rate under a 12h L/D schedule calculated from a published Gro-Seq database (Fang et al., 2014) and BMAL1, CLOCK, PER2, H3K4me3, H3K4me1 and H3K27Ac cistromes (Koike et al., 2012). Amplicons of ChIP-qPCR and regions of RNA for quantification are illustrated by arrows of different color. **(I)** ChIP-qPCR of XBP1s on 4.5S RNA, *Per2* and *Cry2* promoter regions were used as negative controls (n=3). **(J-L)** ChIP-qPCR of XBP1s in 2h Tu-treated MEFs with different siRNA knock-down on *Sec23b* **(J)**, *Eif2ak3* **(K)** and *Hspa5* **(L)** genes (n=3). Data are graphed as the mean ± SEM for glucose and insulin quantification and ChIP-qPCR.

Figure S6. Spatio-temporal coordination of the 12h rhythm of hepatic metabolism, related to Figure 5 and 6.

(A) Key carbohydrate, nucleotide and lipid metabolic pathways having rate-limiting enzymes with 12h oscillations of expression in mouse liver are demonstrated in different colors. The phases of the oscillations of metabolic enzymes in corresponding metabolic

pathways are shown in the bottom right corner. In addition, the phases of the 12h rhythm of mRNA transcription based upon **Figure1 H** are also shown. Black-boxed phases indicate the phase of the larger peak that is often superimposed by the peak of the 24h circadian rhythm. Metabolic pathways lacking black-boxed phases indicate that the two peaks of the 12h rhythm are symmetrical and therefore suggest that they largely lack a superimposed circadian rhythm. Key rate-limiting enzymes with a 12h rhythm are numbered from 1 to 24 and numbers in blue indicate proteins whose corresponding mRNAs do not exhibit ~12h oscillation per the eigenvalue/pencil method. Please be noted that of the 18 NUDF family members, *Ndufa11*, *Ndufab1*, *Ndufb11*, *Ndufb2*, *Ndufb4* and *Ndufc2* do exhibit ~12h oscillation at the mRNA level (See **Table S1**). Further, the sub-cellular localizations (mitochondria, ER or nucleus) of different metabolic pathways are depicted by blue box, red box and yellow circle, respectively. **(B)** 12h rhythm of RBKS mRNA and protein expression is associated with the 12h oscillation of ribose levels in mouse liver. RBKS catalyzes the conversion from D-ribose to D-ribose 5-phosphate (top). Oscillations of *Rbks* pre-mRNA and eRNA transcription (middle left), mature *Rbks* mRNA expression and its eigenvalue/pencil deconvolution (middle right), RBKS protein level (bottom left) and ribose levels (bottom right) in mouse liver. **(C)** 12h rhythm of SUCLA2 mRNA and protein expression is associated with the 12h oscillation of succinyl-CoA level in mouse liver. SUCLA2 catalyzes the conversion from succinyl-CoA to succinate (top). Oscillations of *Sucla2* pre-mRNA transcription (middle left), mature *Sucla2* mRNA expression and its eigenvalue/pencil deconvolution (middle right), SUCLA2 protein level (bottom left) and succinyl-CoA levels (bottom right) in mouse liver. **(D-H)** Mice under *ad libitum* (n=7) or restricted feeding (n=8) conditions are housed in CLAMS system under a 12h L/D schedule. Averaged real-time food intake of mice under *ad libitum* **(D)** or restricted feeding **(E)** conditions. **(F)** Average daily food intake in light (ZT0~12) and dark (ZT12~ZT24) phase for mice housed under *ad libitum* and restricted feeding conditions. **(G-H)** Eigenvalue/pencil method deconvolution of RER data from 7 individual mice housed under *ad libitum* conditions **(G)** and from 8 individual mice housed under restricted feeding conditions **(H)**.

Figure S7. 12h CREMA is conserved in crustaceans and nematodes, related to Figure 7.

(A) RPKM normalized quantification of mouse hepatic mtDNA-encoded RNA synthesis rate under a 12h L/D schedule calculated from published Nascent-Seq dataset (Menet et al., 2012). UCSC genome browser snapshot of Nascent-Seq tracks across the 16.1 kb mouse mitochondrial genome. Protein-coding genes encoded on the positive (H) strand are shown in red while genes on the negative (L) strand are shown in blue. Boxes show UCSC tracks with higher magnification for specific regions. **(B)** mRNA levels of several mtDNA-encoded genes as calculated from a published microarray database (n=5) under a 12h L/D cycle (Eckel-Mahan et al., 2013). The data are double plotted for better visualization. **(C)** qPCR analysis of four mtDNA-encoded genes under constant darkness conditions (n=3~7). **(D)** Raw data and eigenvalue/pencil decomposition of genes involved in mitochondrial gene regulation as calculated from the 48h microarray database (Hughes et al., 2009). **(E)** Log_2 (fold change to mean) for key *C. elegans* ortholog of mammalian 12h cycling ER and metabolism genes under temperature entrainment and free-run conditions. Two independent replicates (corresponding to experiment 3 and 4 in the original study) were shown. **(F)** List of top ten 12h cycling mouse genes identified by the eigenvalue/pencil method and their *C. elegans* orthologs with the status of 12h rhythmicity shown. Only genes with decay rate greater than 0.9 were selected. **(G)** Log_2 (fold change to mean) for *C. elegans* ortholog of mammalian top ten 12h cycling genes under temperature entrainment and free-run conditions. Two independent replicates (corresponding to experiment 3 and 4 in the original study) were shown. **(H)** List of top ten 24h cycling mouse genes identified by the eigenvalue/pencil method and their *C. elegans* orthologs with the status of 24h rhythmicity shown. Only genes with decay rate larger than 0.9 were selected. **(I)** Log_2 (fold change to mean) for *C. elegans* ortholog of mammalian top ten 24h cycling genes under temperature entrainment and free-run conditions. Two independent replicates (corresponding to experiment 3 and 4 in the original study) were shown.